PLANETARY SCIENCE

Core metamorphism controls the dynamic habitability of mid-sized ocean worlds—The case of Ceres

Samuel W. Courville[1,2]*, Julie C. Castillo-Rogez[2], Mohit Melwani Daswani[2], Jordyn Robare[3,4], Joseph G. O'Rourke[1]

Ceres's surface mineralogy and density structure indicate an aqueous past. Observations from the Dawn mission revealed that Ceres likely hosted a global subsurface ocean in its early history, which was the site of pervasive aqueous alteration of accreted material. Subsurface environmental constraints inferred from Ceres's surface mineralogy, combined with Ceres's high abundance of carbon, suggest that the dwarf planet may have been habitable for microbial life. We present a coupled chemical and thermal evolution model tracking Ceres's interior aqueous environment through time. If the rocky interior reached ≳550 K, then fluids released by rock metamorphism would have promoted conditions favorable for habitability by introducing redox disequilibrium into the ocean, a source of chemical energy for chemotrophs. We find that this period would have been between ~0.5 and 2 billion years after Ceres's formation. Since then, Ceres's ocean has likely become a cold, concentrated brine with fewer sources of energy, making it less likely to be habitable at present.

INTRODUCTION

Ceres is a candidate ocean world (*1*). Perhaps more accurately, it could be a residual ocean world—a body that once had a large ocean that has since cooled and nearly frozen completely, leaving behind a concentrated brine (*2*). The NASA's Dawn mission revealed that Ceres's density structure is consistent with a rocky interior covered by a ~50-km-thick ice shell (*3*, *4*). although there are no direct observations that confirm the presence of liquid water today—either as a thin, briny layer beneath the ice or within mantle pore space (*5*)—pervasive aqueous alteration observed in the surface mineralogy (*6*) and the differentiation of an ice shell indicate that Ceres hosted a global ocean early in its history (*7*–*9*). Because of the recent evidence for brines at Ceres (*10*, *11*), a key objective of future spacecraft missions will be to assess the dwarf planet's habitability (*12*).

Even if Ceres does have a brine layer at present-day, however, it may not be habitable. To explain the recent extrusion of sodium chloride at Ceres's Occator crater (*2*), the residual liquid layer within Ceres likely has a temperature between ~210 and 250 K (*13*), which is lower than the coldest known limit for terrestrial microbial life (*14*). Despite these current constraints, the occurrence of vast surface deposits of sodium carbonate and ammonium salts (*15*, *16*) suggests that Ceres hosted a warmer, alkaline subsurface ocean in its past. Ceres's interior was likely warmer in the past from the decay of radioactive isotopes (*17*). Furthermore, organic matter in the regolith (*18*, *19*) could mean that conditions favorable for organic synthesis existed in Ceres's primordial ocean (*13*, *20*, *21*). So, the environmental conditions—i.e., temperature, pressure, pH, and the availability of key elements (*22*)—required for life were likely satisfied in Ceres's early ocean. However, for Ceres's early ocean to sustain life, there must also have been a source of energy for life to exploit (*23*, *24*).

Whether the necessary conditions—whatever they may be—for abiogenesis, the formation of life from nonlife, could have been met in an icy ocean world is an open question (*25*). However, if life were to form on Ceres within a subsurface ocean devoid of light, then it would have been chemotrophic, i.e., using chemical energy from redox disequilibrium to sustain itself (*26*). In this study, we focus on the interior geophysical events that could supply chemical disequilibrium to Ceres's ocean and thus create or sustain habitable environments. We use a combined thermal and chemical model to track Ceres's habitability—assuming that the availability of chemical energy is the limiting factor for Ceres's habitability—over the course of Ceres's internal evolution, specifically evaluating methanogenesis as a potential metabolism. Henceforth, we use the word "evolution" to refer to geophysical change of Ceres's interior over time. The evolution model we present applies for mid-sized icy bodies (e.g., ~500 to 1000 km in diameter) in general. So, icy bodies of similar size to Ceres (~940 km in diameter), i.e., some of the moons of Uranus and Saturn, could have experienced similar internal evolutions (*27*). Thus, our work is important for assessing the dynamical habitability of these types of bodies.

RESULTS

Thermal evolution metamorphoses interior and releases fluids

Ceres's evolution likely involved four major stages: accretion, ice-rock differentiation, rocky core metamorphism, and ocean freezing. These stages are illustrated in Fig. 1, which shows how Ceres's interior temperature evolved over time. Interior heating dictates the compositional changes in Ceres's interior. To match Ceres's density, we assume that the starting composition had the same elemental abundances as 10 weight % (wt %) water ice and 90 wt % carbonaceous, Ivuna-type (CI) chondrite meteorites. CI chondrites contain additional water within hydrated minerals. The hydrated minerals within CI chondrites likely came from aqueous alteration of more primitive matter on their parent bodies (*28*). Similarly, we assume that Ceres accreted primordial matter, such as the precursor material for CI chondrites, and altered it upon reaching a hot enough

[1]School of Earth and Space Exploration, Arizona State University, 781 Terrace Mall, Tempe, AZ 85287, USA. [2]Jet Propulsion Laboratory, California Institute of Technology, 4800 Oak Grove Dr., Pasadena, CA 91011, USA. [3]School of Molecular Sciences, Arizona State University, 781 Terrace Mall, Tempe, AZ 85287, USA. [4]Department of Genome Sciences, University of Washington, 3720 15th Ave NE, Seattle, WA 98195, USA.
*Corresponding author. Email: swcourvi@asu.edu

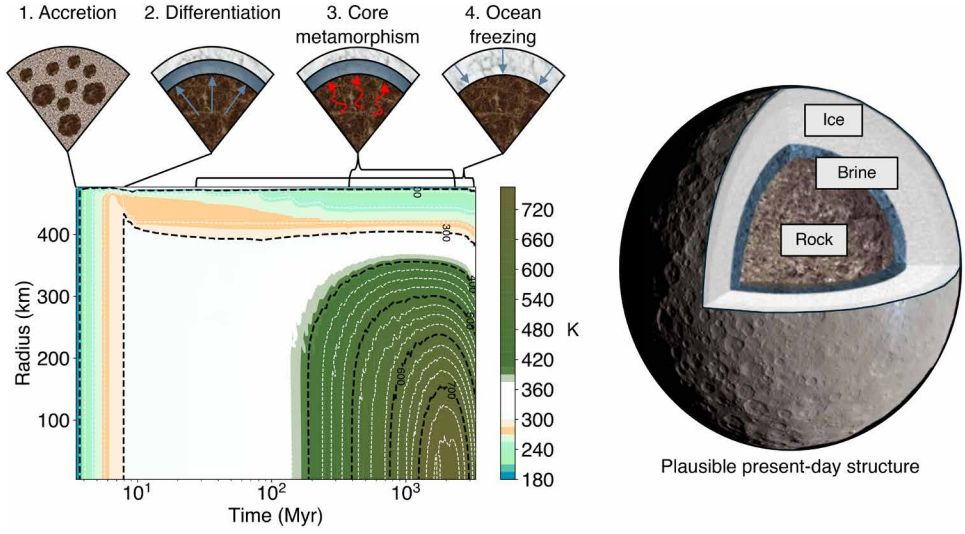

Fig. 1. Ceres's temperature evolution drives major interior events. Depending on the extent of internal heating, a mid-sized (~500- to 1000-km radius) icy body such as Ceres may undergo differentiation and then metamorphism of its interior and ocean freezing, leading to the present-day interior structure. After accreting (1), the temperature within Ceres as a function of time and depth controls the events that determine Ceres's habitability: (2) ice-rock differentiation at ~4 Myr, (3) metamorphic volatiles are added into the ocean ~0.5 to 2 Gyr, and (4) ocean freezing. Here, we assume the ice shell is made of pure water ice.

temperature to melt water ice. We use a thermal evolution model based on literature-predicted values for radioisotope abundances in CI chondrites and Ceres's formation time: 3.5 million years (Myr) after the condensation of CAIs (calcium-aluminum–rich inclusions) (*7*, *17*, *29*, *30*).

The decay heat from ^{26}Al is sufficient to melt the accreted water ice by ~5 Myr after formation, leading to the differentiation of water and rock. While Ceres's rocky mantle continues warming because of long-lived radioisotope decay, the bulk of its shell freezes over a timescale of ~1 billion years (Gyr). The rocky core reaches its peak temperature at ~2 Gyr. The influx of water from the dehydration of hydrated silicates contributes to prolonging the ocean's lifetime. However, the heat flux from Ceres's interior is insufficient to support a global ocean until present day, and the ocean nearly completely freezes by 3.5 Gyr. However, a thin, liquid layer could exist today if it is rich in antifreezes, such as ammonia (*7*).

Figure 2A illustrates how Ceres's core mineralogy evolves over time. The initial water-rock reaction during Ceres's differentiation results in a serpentinized system—a hydrated silicate interior and a reduced ocean. The initial mineralogy consists primarily of hydrated silicates, iron sulfides, and carbonates. When the interior temperature reaches ~550 K, at ~500 Myr, silicates begin to dehydrate, marking the onset of thermal metamorphism. Only the deeper interior dehydrates, whereas shallower, cooler depths remain hydrated. Silicates continue to dehydrate until the peak temperature of ~800 K at 2 Gyr. Minor carbonate decarbonation begins at ~700 K, releasing carbon dioxide. Figure 2B displays the mass of fluid released due to metamorphism. Initially, the water-rock reactions between the accreted ice and rock determine the ocean's composition (*6*, *7*). As the ocean freezes (Fig. 2C), the concentrations of solutes increase (Fig. 2D).

Chemical disequilibrium from metamorphism could support microbial metabolisms

Fluid that equilibrated deeper within Ceres's interior, e.g., in the deepest pore space ~150 km beneath the sea floor (Fig. 3A), has a different solute composition compared to the seafloor. Higher temperature fluids favor CO_2 formation over CH_4 (*31*). Thus, at equilibrium, the higher temperature in deep pore space (Fig. 3B) produces greater concentrations of dissolved CO_2 and H_2 compared to the seafloor (Fig. 3C). Deep pore fluid would be out of equilibrium with conditions predicted for the seafloor. As deep pore water moves upward toward the colder seafloor, the reduction of CO_2 to CH_4 becomes favorable (*31*). However, at low temperature, the kinetics of uncatalyzed reduction of oxidized carbon species is slow (*32*). For life to take advantage of the reaction, the reaction's abiotic rate must be slower than the rate at which fluid is supplied to the ocean.

The energy available for the reduction of CO_2 to CH_4, i.e., methanogenesis, depends on the extent of the reaction's disequilibrium and the availability of the reaction's limiting reactant. Figure 3D displays the energy supply implicit in re-equilibrating the fluid from the deepest pore space 150-km beneath the seafloor at the temperature and pressure of the seafloor (see Materials and Methods). The number of microbial cells that this energy supply could support depends on the demand of a given cell, which varies by cell type and environment. However, for context, we adopt a previously published maintenance energy for anaerobic cells: 3.7×10^{-15} J per cell s^{-1} (*33*–*35*). Under this assumption, a flow of 1 kg s^{-1} of deep pore fluid migrating to the seafloor could support ~3×10^{15} cells. Thus, the size of the potential biosphere would depend on the flow of fluids from depth. However, the exact maintenance energy for a cell depends on the specific cell and its environment and may vary by orders of magnitude. Furthermore, the precise supply of energy that would be available to a microbe would depend on many factors: the depth and temperature at which the deep fluid last equilibrated; the rate and mixing ratio at which hydrothermal fluids are added to the ocean; and the temperature and depth at which the methanogenic microbial communities may be located. Since we highlight the fluid composition that would yield the maximum chemical disequilibrium, the energy values we provide in Fig. 3D should be interpreted as an

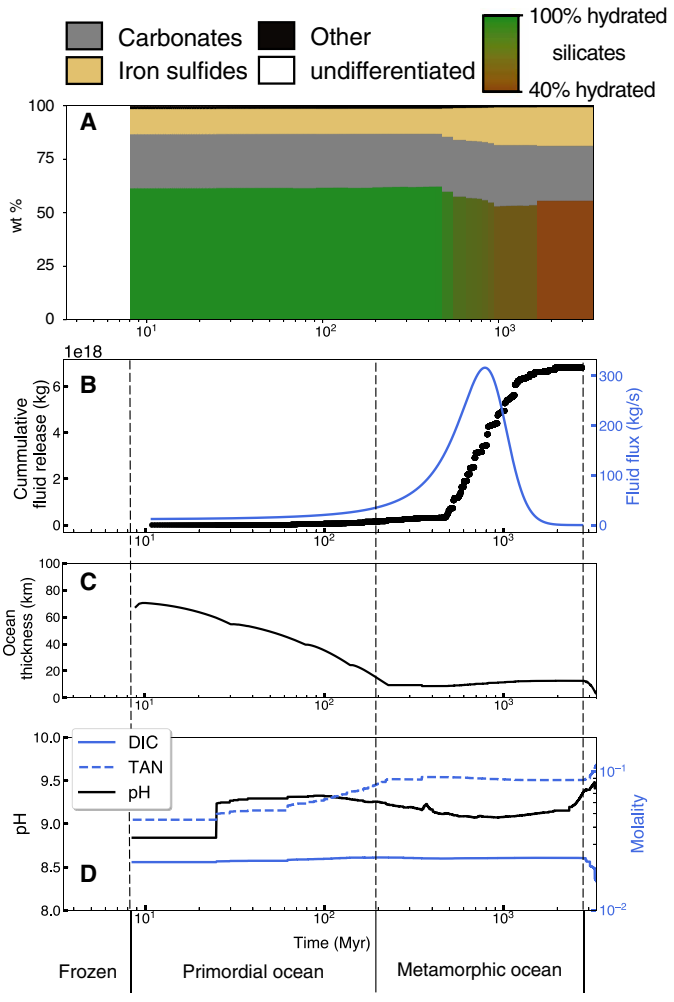

Fig. 2. Cere's core undergoes thermal metamorphism, releasing volatiles. (**A**) Ceres's core mineral phase assemblage evolution over time leads to the release of volatiles as a consequence of silicate dehydration and carbonate decarbonation. See fig. S2 for the complete predicted mineral phase assemblage. (**B**) Cumulative fluid release from all depths in the interior (left axis) and the smoothed rate of fluid release (right axis). (**C**) Thickness of Ceres's ocean over time. (**D**) Ocean pH (left axis) and the molalities (right axis) of dissolved inorganic carbon (DIC) and total ammoniated nitrogen (TAN). See figs. S4 and S5 for complete plots of all solutes.

order-of-magnitude upper bound that primarily illustrates the temporal trend of energy availability in Ceres.

DISCUSSION

Availability of chemical energy controls duration of habitability

Metamorphism of rocky interiors could be a major stage of icy body evolution (*5*, *27*, *36*). For Ceres, metamorphism would have lasted hundreds of millions of years. Hydrothermal fluids released from silicate dehydration that equilibrated in deep pore space could supply chemical redox disequilibrium to Ceres's ocean, in a way similar to some terrestrial systems (*37*, *38*). We find that Ceres's deep pore fluids would have higher concentrations of H_2 and CO_2 compared to the ocean. Consistent with results from a previous study (*31*), we find that the abundance of H_2 limits the potential for methanogenesis. Thus, Ceres's most habitable period would have been during metamorphism, between ~0.5 and 2 Gyr after formation. Peak energy availability would occur when Ceres reached its peak temperature at ~2 Gyr.

For life to exploit the potential chemical energy from deep pore fluids, there would have to be fluid flow from deep pore space to the seafloor. The rate of fluid flow would affect the potential biomass that could be supported. During the peak of silicate dehydration, the fluid flow could reach over 300 kg s^{-1}. Given our previous estimate of the number of cells that fluid flow could support (~3×10^{15} cells per kg s^{-1}), ~300 kg s^{-1} of fluid flow corresponds to a peak, order-of-magnitude biomass of ~10^{17} cells. For a given mass of ocean water, this number of cells would have equated to a cell concentration of ~10^3 cells kg^{-1}, assuming that the cells were spread evenly

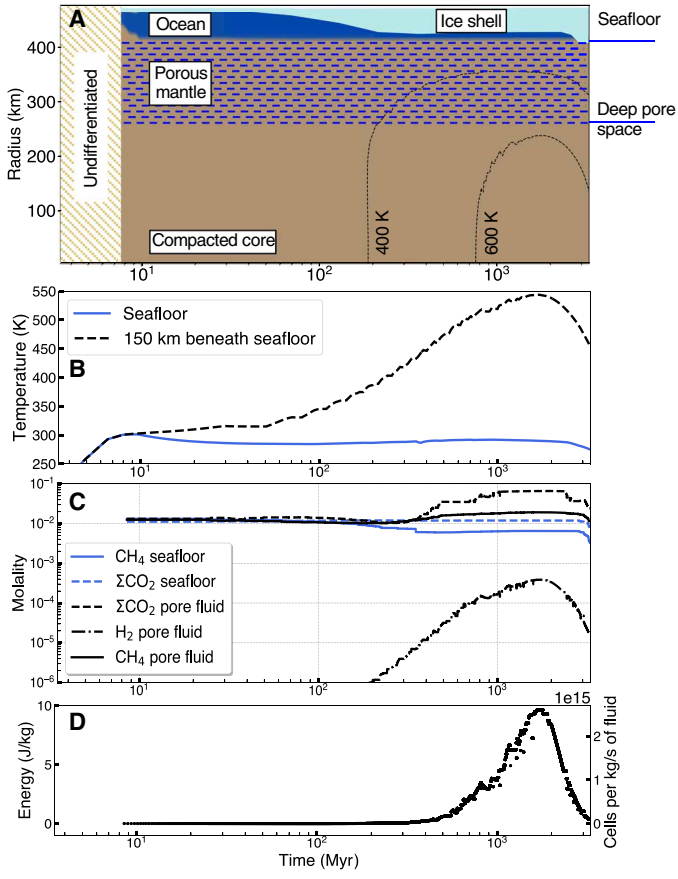

Fig. 3. Thermal metamorphism of the deep interior produces an extended period of redox disequilibrium between ocean and pore fluids. (**A**) Ceres's structure over time. Fluid within deeper pore space experiences higher temperatures than the seafloor (**B**). Differing temperature and pressure conditions produce different equilibrium fluid compositions between the seafloor and the deep pore fluid (**C**). The difference between Ceres's ocean and deep pore fluid is greatest during the warmest period of Ceres. (**D**) Chemical energy supply from methanogenesis (left axis) that deep pore fluid could provide when brought to the temperature and pressure of the seafloor, along with a corresponding number of cells that could be sustained by this energy supply (right axis).

throughout a global, 1-m-thick layer of ocean water on the Cerean seafloor. This value is much less than the ~10^9 cells kg^{-1} one might expect at Earth's seafloor (*39*). Greater fluid flow or locally concentrating the fluid flow would support a denser biological community. Fluid flow could increase if hydrothermal circulation recycled ocean water into deep pore fluids that subsequently heated and returned to the seafloor. However, too much hydrothermal circulation would extract heat from the core (*40*, *41*) and extinguish the habitability potential. Thus, the best habitability case for a dwarf planet such as Ceres might be a modest amount of hydrothermal fluid flow, coalescing into fracture conduits, and localized vent systems that release H_2-rich fluid at the rate of tens to hundreds of kilograms per second.

The distance that fluid from Ceres's rocky core must travel to reach the ocean is much greater than that of analogous hydrothermal systems on Earth. On Earth, even relatively cool seafloor hydrothermal systems, such as the Lost City, have steep thermal gradients compared to our model of Ceres (*42*). Fluids at Lost City need only hydrothermally circulate at depths of perhaps a few kilometers beneath the ocean floor. On Ceres, hydrothermal fluids with similar redox disequilibrium as terrestrial vent systems would need to originate at depths of many tens of kilometers. Fluid migrating upward at that scale could take thousands of years depending on the permeability of the system (see Fig. 4A) (*40*, *43*). The chemical energy released to the ocean depends on Ceres's core porosity and permeability. If fluid took longer to reach the ocean than for the fluid to chemically equilibrate, then there would not be any energy available for life. Figure 4A demonstrates that if Ceres had a highly permeable interior, as would be the case if it were fractured from volume changes (*44*), then fluid could flow from the deepest pore space ~150 km beneath the ocean upward to the ocean in a matter of years, whereas the equilibration timescale would be on the order of 100 years. This scenario would provide the maximum amount of chemical energy, as plotted in Fig. 3D. However, if Ceres had a less permeable interior, then the fluid may take ~1 kyr to ascend, much slower than the equilibration timescale at 150 km below the ocean floor. The depth that the fluid last equilibrated would therefore depend on the permeability of the interior. Figure 4 (B and C) shows how the chemical energy changes as a function of the equilibration depth. We note, however, that there are other redox reactions that consume hydrogen, so the

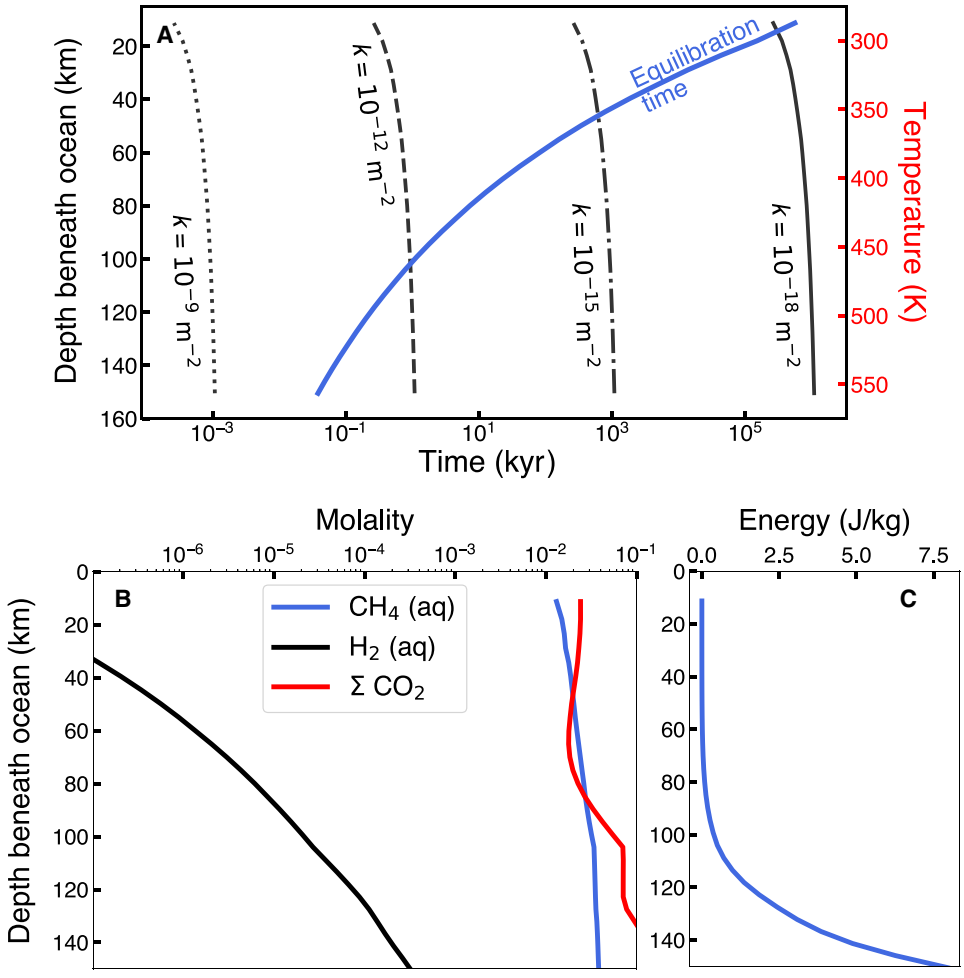

Fig. 4. Chemical energy depends on the relative rates of fluid flow versus chemical equilibration. Corresponding to the temperature and porosity in our model at 1.5 Gyr after Ceres's formation, (**A**) displays the time required for fluid to flow from a given depth beneath the ocean to the ocean for four different permeability values (black lines) and the chemical time constant for equilibrating CH_4 and CO_2 (blue line). (**B**) Equilibrium concentrations of each relevant species as a function of depth. (**C**) Energy available by equilibrating (quenching) a fluid from a given depth after it has moved to the conditions at the sea floor.

equilibration timescale of methanation may not be representative of the system. Thus, our energy values should be considered an upper bound for methanogenesis.

We demonstrate that rocky core metamorphism can supply chemical energy over geologic timescales. However, the precise chemical energy supply that may have existed within Ceres depends on Ceres's interior composition and peak core temperature, which are uncertain. To first order, the most important parameter is the amount of internal heating within Ceres; the hotter the interior, the more disequilibrated fluid the interior releases into the ocean (fig. S1). Furthermore, when hydrothermal fluids enter Ceres's ocean or pore space, they would form buoyant plumes that rapidly entrain ambient water (*45*). This entrainment creates concentration gradients that diminish with distance from vent sources. As a result, the potential for biomass production would be highest near hydrothermal outlets, decreasing in the broader ocean and pore space. Our calculations provide estimates of the total energy availability, while the precise distribution of habitable zones would be shaped by local fluid dynamics. Future studies should jointly quantify the rate of fluid circulation through pore space and the flux of energy for methanogenesis over time at varying rates and depths of fluid mixing. To fully map the possible energy supplies from core metamorphism, one must consider the entire parameter space of possible compositions, permeabilities, potential metabolisms, and kinetic rates.

Alternative sources of energy could influence habitability

In this study, we have focused on the energy available from hydrothermal fluids from Ceres's interior. However, there are other potential sources of oxidants and reductants that could supply energy for life. Solar radiation produces oxidants on the surface that may be a source for redox disequilibrium in the ocean if there are mechanisms to deliver the oxidants to the ocean, such as large impacts, which could breach the ice shell and deliver surface material to the ocean (*13*, *46*). However, this mechanism would be a stochastic process that likely could not sustain habitability for a long period if impacts were not sufficiently frequent and well-distributed over Ceres's surface. Alternatively, ice shell convection could recycle surface material to the ocean (*24*, *46*–*49*). However, the heavily cratered surface of Ceres implies that no convection is occurring now or within the past ~1 Gyr (*50*).

As another potential energy source, the radiolysis of water could create redox disequilibrium (*51*). The production of H_2 from radiolysis would likely be <1 nmol year^{-1} (*13*). Radiolysis would, therefore, not produce high concentrations of H_2, such as the ~10 μmol of H_2 that we predict in our modeled metamorphic fluids. This is to say, that although the radiolytic production could possibly be spread uniformly over the entire ocean volume and accumulate to more H_2 produced than that released by hydrothermal fluids, there would never be a high concentration of H_2 at one time or location. Nevertheless, radiolysis-driven life exists on Earth (*52*, *53*), so radiolysis is a plausible energy source for life on Ceres. In any case, we argue that the absence of thermal metamorphism in Ceres's core would decrease the overall habitability potential of the dwarf planet, in comparison to evolution pathways that allowed for metamorphism.

Alternative interior conditions may alter habitability

We find that core metamorphism may be required for bodies such as Ceres to host extended periods of habitability. Although observations suggest that Ceres is partially differentiated (*4*), uncertainties in Ceres's bulk composition, thermal and physical properties, and accretion time preclude a conclusive assessment of the peak temperature reached within Ceres's core. Furthermore, the likely presence of a large fraction of porosity in the upper core compounded with the large uncertainty in the core density (*5*) prevents ascertaining whether Ceres's core underwent thermal metamorphism. Regardless of the true extent to which Ceres was thermally processed, the sequence of major evolution events we highlight in Fig. 1 are general processes that may occur for mid-sized (500- to 1000-km radius) bodies.

As previously stated, whether Ceres's underwent metamorphism depends on Ceres's peak temperature. In turn, the peak temperature that Ceres's interior reaches depends on Ceres's composition. However, Ceres's initial composition is uncertain. Formation models suggest that it could have accreted between the orbits of giant planets from material resembling CI chondrites (*54*). Most large bodies in the outer solar system likely accreted a fraction of cometary material, too (*55*). A CI chondrite–like composition implies that Ceres accreted with mostly silicate rocks and water ice. In contrast, a cometary composition involves up to ~40 wt % macromolecular organics and ~10 wt % nonwater cometary ices such as CO_2, CO, CH_4, and NH_3 (*36*). If Ceres formed with a large fraction of organic matter (*56*, *57*), then there would be three main consequences: The refractory core would be larger than in our models because organic matter is less dense than silicate rocks; the ocean/ice shell would consequently be thinner; and the interior would produce less heat because the high abundance of organic matter would reduce the relative abundance of radioisotopes (*58*). Variations in the initial abundance of potassium controls the peak core temperature and release of metamorphic fluids (fig. S1). However, we note that these alternative compositions would also produce interior mineral assemblages with different thermal conductivities. A higher thermal conductivity would reduce the peak interior temperature. Reduced heating or increased thermal conductivity may preclude metamorphism of Ceres's interior, thereby reducing Ceres's habitability potential.

We find that the concentration of H_2 in the metamorphic fluid is the limiting reactant for methanogenesis within Ceres. In general, the energy supply increases with the abundance of H_2, and the abundance of H_2 increases with temperature (Fig. 4B). However, the rock composition and the water-rock mass ratio also control the production of H_2. For example, a study of ultramafic rock alteration has shown that at 550 K, and the activity of aqueous H_2 may vary between 10^{-6} and 10^{-1}, increasing as the water-rock ratio decreases and varying depending on the relative abundances of Fe, Mg, and Ca (*59*). Thus, if Ceres has a different bulk composition than our CI chondrite–like assumption, then there may be a different hydrogen abundance. Regardless, the trend of energy availability would be the same, with a peak in energy availability during core metamorphism.

Future exploration could uncover evidence of interior metamorphism

Since Ceres is not subject to as many complex evolutionary factors (e.g., tidal heating) as are many other candidate ocean worlds that orbit gas giants, it is an ideal body to study evolutionary pathways relevant to candidate ocean worlds in the ~500- to 1000-km radius range. Being in large numbers, these bodies might represent the most abundant type of habitable environment in the early solar system. From a chemical energy perspective, the most habitable periods for these objects were when the rocky interiors underwent thermal

metamorphism. Metamorphism leads to an influx of fluids into the ocean. These fluids could provide a steady source of chemical disequilibrium for several hundred million years. In the case of Ceres, the metamorphic period between ~0.5 and 2 Gyr would have created a potentially habitable environment at the seafloor if the rocky mantle reached temperatures greater than ~700 K. The decreasing temperature of Ceres's interior over the past ~1 Gyr would likely render it thermodynamically inactive at present.

A future sample return mission to Ceres's evaporites, which is a mission theme recommended in the Origins, Worlds, and Life decadal survey (*60*), should aim to investigate the signatures of past habitability by seeking to answer whether core metamorphism influenced Ceres's brine fluid composition. This information might be found in carbon isotopic ratios in exposed carbonates or within salt crystals on Ceres's surface that may have trapped fluids from Ceres's deep interior (*61*).

MATERIALS AND METHODS

Combined thermal and chemical evolution

We model Ceres's interior evolution using a fully coupled thermal and chemical evolution code. Figure 5 displays the flow of the code. During each time step, the code updates the interior's composition and temperature. The temperature change can affect the composition, and the composition change can affect the temperature.

We use a heat conduction equation to model the temperature within Ceres. At a given time step, *i*, and radial position, *r*, the equation

$$\frac{d\left[\frac{k_{i,r}(T)dT(r)}{dr}\right]}{dr}+\frac{2}{r}\frac{k_{i,r}(T)dT(r)}{dr}=\rho_{i,r}C_{p(i,r)}(T)\frac{dT(r)}{dt}-H_{i,r}(t)-L_{i,r} \quad (1)$$

describes the temperature evolution of the interior, where T is the temperature (K), r is the radius (m), k is the thermal conductivity (W m^{-1} K^{-1}), ρ is the density (kg m^{-3}), C_p is the specific heat capacity (J K^{-1} kg^{-1}), H is radiogenic heat, and L is the latent heat from ice freezing/melting and/or mineral phase changes (*27*). Radiogenic heat is

$$H(t)=mW_0\exp\left(-\frac{\ln 2\, t}{t_{\frac{1}{2}}}\right)dt \quad (2)$$

where m is the mass fraction of a given radioisotope, $t_{1/2}$ is its half-life, and W_0 is the specific heat production from radiogenic decay of the given radioisotope (W kg^{-1}). The model is one-dimensional and assumes spherical symmetry. We solve this equation with a finite difference scheme where we determine the time step, *dt*, using the Courant-Friedrichs-Lewy condition (*62*)

$$2\kappa\Delta t=\Delta r^2 \quad (3)$$

where κ is thermal diffusivity, $\kappa=\frac{k}{\rho\, C_p}$. Because the thermal conductivity varies as a function of temperature and composition, the time step is different at different times and radial positions. So, we set the time step at each time based on the radial position with the shortest necessary time step. The radius step, *dr*, is variable. We set each radius step to contain a constant mass, so the radius step distances changes depending on the density of the interior.

The density, heat capacity, thermal conductivity, latent heat, and specific heat production are composition dependent (see fig. S2 for our model's density, heat capacity, thermal conductivity, and porosity). We determine the composition with Gibbs free energy minimization (see section below). In addition, we determine volatile evolution with three simple rules: (i) fluids differentiate from the rocky core; (ii) as fluids are released, the rock core compresses; and (iii) fluids

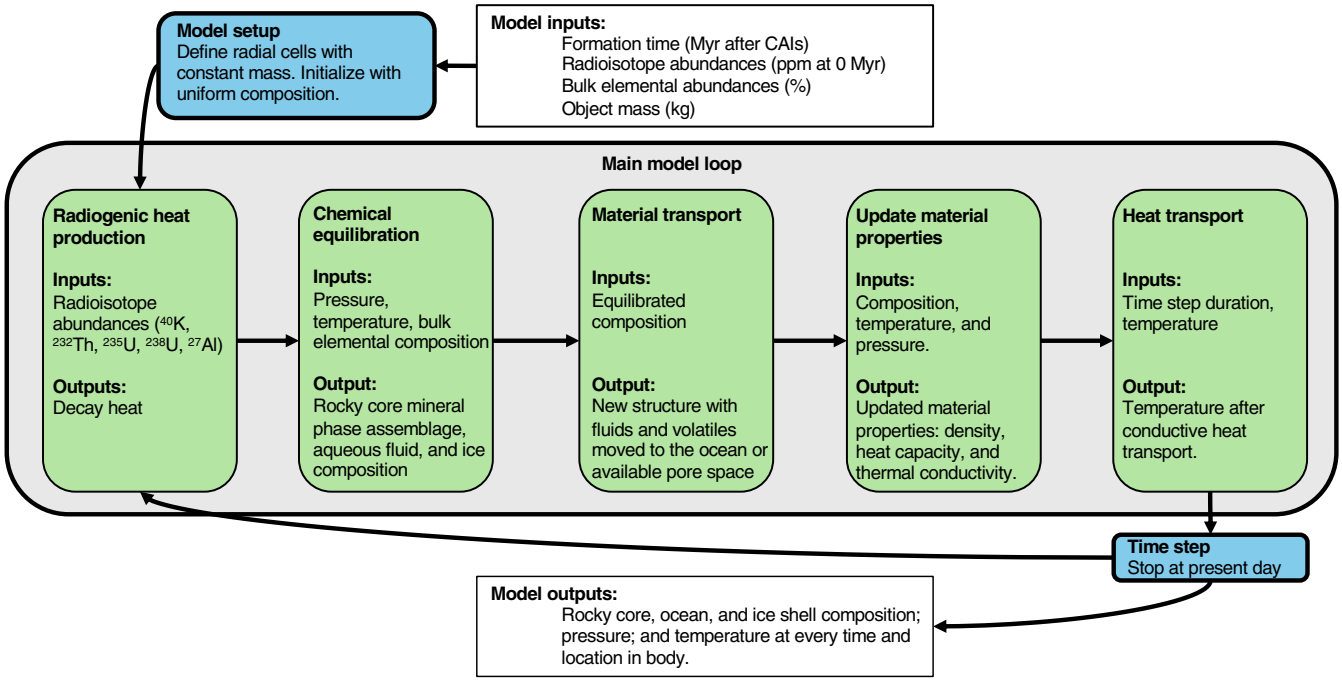

Fig. 5. Flowchart of the modeling procedure. This flowchart illustrates how we model the coupled thermal and compositional evolution of Ceres.

mix fully. We assume porosity in the rocky mantle evolves as a function of pressure

$$\phi = \phi_{max}\, e^{-\frac{cP}{P_c}} \quad (4)$$

where P is pressure; ϕ_{max} is the maximum porosity at zero pressure, which we assume to be 0.4; $c \sim 6$ is a constant; and P_c is the pore closure pressure, which we set at 100 MPa (*63*). Porosity can also depend on the temperature of the environment. Increasing temperature can facilitate the viscous closure of pore space. However, we do not model this process, as it most notably occurs at temperatures above ~650 K (*64*), which is greater than the temperature in the deepest pore space of our model.

We calculate flow timescales as a function of permeability for different depths beneath Ceres's ocean assuming Darcy flow. As modeled in (*36*), flow velocity, v, is given by

$$v(z) = \frac{k}{\mu\phi}\frac{dP}{dz} \quad (5)$$

where k is permeability, μ is the fluid viscosity, ϕ is porosity, P is pressure, and z is depth. This plot assumes a lithostatic pressure gradient where Eq. 4 determines ϕ.

We assume that Ceres's ocean would remain isothermal and instantly transfer heat from the seafloor to the base of the ice shell. Thus, the ocean remains near freezing as it efficiently transfers heat to the overlying ice shell. We include the latent heat of freezing ice in our thermal model, so ice freezing moderates the thickness of the ocean. The decay of radioactive isotopes is the primary heat source. We assume heat conduction through the ice shell. The viscosity of pure ice may allow for thermal convection if there is sufficient heat flow (*65*). However, we choose not to include convective heat transfer because there is no evidence for ice shell convection on Ceres's surface. Furthermore, recent studies suggest that Ceres's ice shell has increasing impurities with depth and greater strength than expected for pure ice (*9*, *66*). A compositional gradient and impure ice would inhibit convection. If ice shell convection did occur on Ceres, then the ocean would freeze faster.

We calculate interior heating within silicate rocks using the radioactive isotope abundances listed in Table 1, which are based on the elemental abundances in CI chondrites (*67*, *68*). Two isotopes largely determine Cere's temperature: ^{26}Al and ^{40}K (see fig. S3 for their abundances in Ceres over time). Because CI chondrites themselves are pervasively aqueously altered, the abundance of potassium in these meteorites should be representative of that which our models assume for Ceres after differentiation. Any further leaching of potassium into the ocean, which we do not model, would reduce the rate of heating in the core and create a heat source in the ocean.

During metamorphism, the mass of fluids released is small compared to the mass of the core and ocean (Fig. 2). Thus, any heat transport from these fluids would not affect the overall thermal structure predicted by our model. However, sustained hydrothermal convection of fluids in the porous mantle could extract much more heat (*40*). Thus, fluid convection is a double-edged sword; sustained hydrothermal convection could increase available energy for life in the ocean, but only if it does not reduce the peak interior temperature to the point where there is insufficient disequilibrium. Future work could determine the optimal rate of fluid convection for habitability.

Core mineral assemblage modeling

We use the thermodynamic equilibrium software packages Perple_X and Rcrust to model the core mineralogy of Ceres (*69*, *70*). The Supplementary Materials include plots of the full mineralogy (fig. S4). Past studies have used these software packages to predict interior compositions (*5*, *36*). The program takes a list of elemental abundances as input and outputs the mineral phase assemblage with the lowest Gibbs free energy. When Perple_X predicts a change in mineral phase assemblage, we calculate the difference in enthalpy from the new mineral assemblage and the previous assemblage. This enthalpy change is incorporated into Eq. 1 as the latent heat term, L. We use the heat capacities and densities predicted by Perple_X to update the thermal model properties. For most minerals, Perple_X uses a polynomial fit (*71*) for heat capacity

$$C_P = c_1 + c_2 T + c_3 T^{-2} + c_4 T^2 + c_5 T^{-\frac{1}{2}} + c_6 T^{-1} + c_7 T^{-3} + c_8 T^3 \quad (6)$$

and a modified Tait equation of state (*72*) for molar volume

$$\frac{V}{V_0} = 1 - a\left[1 - (1+bP)^{-c}\right] \quad (7)$$

from which one can calculate density. The thermodynamic data file that contains the heat capacity and molar volume coefficients that we use is available within the GitHub repository. We base thermal conductivities on measured values for olivines and serpentines (*73*), where we assign clay and hydrated mineral assemblages a thermal conductivity of 2.5 W m^{-1} K^{-1}, and anhydrous mineral assemblages a thermal conductivity of $k = 1.1 + \frac{600}{T}$. We assign ice a thermal conductivity of $k = 0.4685 + \frac{488.12}{T}$. We assume the thermal conductivity of a mix of multiple components is the weighted average of the components' conductivities. Before water-rock differentiation, we assume Ceres's has a uniform bulk density of 2080 kg m^{-3}, a uniform heat

Table 1. Radioisotope abundances. Present-day isotope fraction of element, starting radioisotope abundances in parts per billion (ppb) relative to the mass of the rock phase, half-lives, and specific heat productions of the radioisotopes in this study.

Isotope	Isotope fraction at present day	Starting abundance (ppb)	Half-life (Myr)	Specific heat production (W/kg)
^{26}Al	0%	377	0.72	0.357
^{40}K	0.0119%	795	1,280	29.17×10^{-6}
^{235}U	0.71%	5	70.4	568.7×10^{-6}
^{238}U	99.29%	16	447	94.65×10^{-6}
^{232}Th	100%	37	14,000	26.38×10^{-6}

capacity of 1000 J kg^{-1} K^{-1}, and a uniform thermal conductivity of 0.5 W m^{-1} K^{-1}. These starting values do not change the late-stage evolution of Ceres, rather they control the time of water-rock differentiation along with Ceres's formation time and ^{26}Al content. Table 2 lists the elemental abundances that we assume for Ceres's starting composition. The software allows for C-O-H-S fluids (*74*). If the software predicts fluids within the equilibrium assemblage, such as water from the dehydration of phyllosilicates, then we transport these fluids upward into available pore space or into the ocean.

Aqueous speciation and chemical energy modeling

The water-rock reactions during differentiation control the composition of the primordial ocean. However, subsequently, the ocean composition evolves as a function of added volatiles from metamorphism and equilibration with the seafloor. Geochemical thermodynamic equilibrium modeling (*75*) predicts the abundance of aqueous species in solution following these water-rock reactions. We use the geochemical modeling software EQ3/6 (*76*), version 8.0a, to predict fluid compositions. The thermodynamic data are sourced from SUPCRT92 (*77*). Although we do not include chloride in the mineral phase modeling, consistent with past studies (*27*), we assume that the water initially contains dissolved chloride (0.0141 wt %) (*78*), which is important to include due to its impact on pH. After each addition of metamorphic volatiles, we re-equilibrated the ocean. We assume that the ocean freezes as pure water ice, resulting in the ocean becoming increasingly enriched in solutes as it freezes (*7*). For all reactions, we assume the water-to-rock mass ratio is 1. See figs. S5 and S6 for plots of all solutes at two different depths within our model.

Chemical energy can be calculated for a specific metabolism by starting with the formula for chemical affinity, given by

$$A = RT \ln\left(\frac{K}{Q}\right) \tag{8}$$

where K is the equilibrium constant at a specified temperature and pressure, Q is the reaction quotient for species in the reaction, R is the ideal gas constant, and T is temperature (*33*). We use Eq. 8 to calculate A for methanogenesis in units of Joule per mole of reaction. The balanced reaction is

$$CO_2 + 4H_2 \rightarrow CH_4 + 2H_2O \tag{9}$$

The equilibrium constant for this reaction varies as a function of temperature. If deep pore fluid ascends to the seafloor without re-equilibrating, then the reaction above would be out of equilibrium. In which case, we evaluate Eq. 8 using the equilibrium constant, K, at seafloor conditions, and the activity product or reaction quotient, Q, as given by the ratios of the reactant species in the pore fluid. The total energy per kilogram of fluid for the given reaction is

$$E_r = \frac{A_r\, m_{\mathrm{lim}}}{S_{\mathrm{lim}}} \tag{10}$$

where m_{lim} is the molality of the limiting reactant in the system and S_{lim} is its stoichiometry (*79*). In the case of methanogenesis in our models, the limiting reactant is always H_2, which has a stoichiometric coefficient of 4. The number of cells which can be supported by a given energy is

$$N_c = \frac{E_r}{E_M}\nu \tag{11}$$

where E_M is the maintenance energy of a cell and ν is the flow of fluid in kilograms per second (*33*). We use a maintenance energy of 3×10^{-15} J $cell^{-1}$ s^{-1} (*34*, *35*), which is appropriate for anaerobic microbes. However, the energy required to build a cell is greater (*80*).

The reduction of CO_2 to CH_4 is kinetically inhibited at low temperatures. We approximate the time constant of this reaction, $\tau = \frac{1}{k'}$, where the pseudo first-order rate constant k' is

$$\log_{10} k' = 6.53 - \frac{4440}{T} \tag{12}$$

and T is temperature in K (*81*, *82*). Equation 9 represents one possible redox reaction that consumes H_2. However, there are many others that can use H_2, and thus, other redox pairs may exhaust the supply of H_2 before methanation, depending on their relative rates.

Table 2. Starting elemental abundances. Bulk elemental abundances for 90 wt % CI chondrites and 10 wt % H_2O.

Element	Abundance (wt %)
H	2.919
C	3.194
N	0.271
O	51.024
Na	0.458
Mg	8.794
Al	0.780
Si	9.822
S	4.911
Ca	0.845
Fe	16.982
K*	0.055
Cl†	0.014

*Included in radioisotope calculations, but not within mineral assemblages or within aqueous speciation. †Included in aqueous speciation, but not mineral assemblages.

Supplementary Materials

This PDF file includes:

Figs. S1 to S6

REFERENCES AND NOTES

1. A. R. Hendrix, T. A. Hurford, L. M. Barge, M. T. Bland, J. S. Bowman, W. Brinckerhoff, B. J. Buratti, M. L. Cable, J. Castillo-Rogez, G. C. Collins, S. Diniega, C. R. German, A. G. Hayes, T. Hoehler, S. Hosseini, C. J. A. Howett, A. S. McEwen, C. D. Neish, M. Neveu, T. A. Nordheim, G. W. Patterson, D. A. Patthoff, C. Phillips, A. Rhoden, B. E. Schmidt, K. N. Singer, J. M. Soderblom, S. D. Vance, The NASA roadmap to ocean worlds. *Astrobiology* **19**, 1–27 (2018).
2. M. C. De Sanctis, G. Mitri, J. Castillo-Rogez, C. H. House, S. Marchi, C. A. Raymond, Y. Sekine, Relict ocean worlds: Ceres. *Space Sci. Rev.* **216**, 60 (2020).
3. A. I. Ermakov, R. R. Fu, J. C. Castillo-Rogez, C. A. Raymond, R. S. Park, F. Preusker, C. T. Russell, D. E. Smith, M. T. Zuber, Constraints on Ceres' internal structure and evolution from its shape and gravity measured by the Dawn spacecraft. *J. Geophys. Res. Planets* **122**, 2267–2293 (2017).
4. R. S. Park, A. S. Konopliv, B. G. Bills, N. Rambaux, J. C. Castillo-Rogez, C. A. Raymond, A. T. Vaughan, A. I. Ermakov, M. T. Zuber, R. R. Fu, M. J. Toplis, C. T. Russell, A. Nathues, F. Preusker, A partially differentiated interior for (1) Ceres deduced from its gravity field and shape. *Nature* **537**, 515–517 (2016).

5. M. Melwani Daswani, J. C. Castillo-Rogez, Porosity-filling metamorphic brines explain Ceres's low mantle density. *Planet Sci. J.* **3**, 21 (2022).
6. M. C. De Sanctis, E. Ammannito, A. Raponi, S. Marchi, T. B. McCord, H. Y. McSween, F. Capaccioni, M. T. Capria, F. G. Carrozzo, M. Ciarniello, A. Longobardo, F. Tosi, S. Fonte, M. Formisano, A. Frigeri, M. Giardino, G. Magni, E. Palomba, D. Turrini, F. Zambon, J.-P. Combe, W. Feldman, R. Jaumann, L. A. McFadden, C. M. Pieters, T. Prettyman, M. Toplis, C. A. Raymond, C. T. Russell, Ammoniated phyllosilicates with a likely outer Solar System origin on (1) Ceres. *Nature* **528**, 241–244 (2015).
7. J. Castillo-Rogez, M. Neveu, H. Y. McSween, R. R. Fu, M. J. Toplis, T. Prettyman, Insights into Ceres's evolution from surface composition. *Meteorit. Planet. Sci.* **53**, 1820–1843 (2018).
8. E. Ammannito, M. C. DeSanctis, M. Ciarniello, A. Frigeri, F. G. Carrozzo, J.-P. Combe, B. L. Ehlmann, S. Marchi, H. Y. McSween, A. Raponi, M. J. Toplis, F. Tosi, J. C. Castillo-Rogez, F. Capaccioni, M. T. Capria, S. Fonte, M. Giardino, R. Jaumann, A. Longobardo, S. P. Joy, G. Magni, T. B. McCord, L. A. McFadden, E. Palomba, C. M. Pieters, C. A. Polanskey, M. D. Rayman, C. A. Raymond, P. M. Schenk, F. Zambon, C. T. Russell, Distribution of phyllosilicates on the surface of Ceres. *Science* **353**, aaf4279 (2016).
9. I. F. Pamerleau, M. M. Sori, J. E. C. Scully, An ancient and impure frozen ocean on Ceres implied by its ice-rich crust. *Nat. Astron.* **8**, 1373–1379 (2024).
10. O. Ruesch, T. Platz, P. Schenk, L. A. McFadden, J. C. Castillo-Rogez, L. C. Quick, S. Byrne, F. Preusker, D. P. O'Brien, N. Schmedemann, D. A. Williams, J.-Y. Li, M. T. Bland, H. Hiesinger, T. Kneissl, A. Neesemann, M. Schaefer, J. H. Pasckert, B. E. Schmidt, D. L. Buczkowski, M. V. Sykes, A. Nathues, T. Roatsch, M. Hoffmann, C. A. Raymond, C. T. Russell, Cryovolcanism on Ceres. *Science* **353**, aaf4286 (2016).
11. M. C. De Sanctis, E. Ammannito, A. Raponi, A. Frigeri, M. Ferrari, F. G. Carrozzo, M. Ciarniello, M. Formisano, B. Rousseau, F. Tosi, F. Zambon, C. A. Raymond, C. T. Russell, Fresh emplacement of hydrated sodium chloride on Ceres from ascending salty fluids. *Nat. Astron.* **4**, 786–793 (2020).
12. J. Castillo-Rogez, M. Neveu, V. Vinogradoff, K. E. Miller, M. M. Sori, F. Tosi, B. Schmidt, J. E. C. Scully, M. Melwani Daswani, K. Hughson, H. McSween, C. De Sanctis, L. Quick, A. Ermakov, G. Thangjam, K. Otto, K. Krohn, P. Schenk, A. Nathues, C. Raymond, Science drivers for the future exploration of Ceres: From solar system evolution to ocean world science. *Planet Sci. J.* **3**, 64 (2022).
13. J. C. Castillo-Rogez, M. Neveu, J. E. C. Scully, C. H. House, L. C. Quick, A. Bouquet, K. Miller, M. Bland, M. C. De Sanctis, A. Ermakov, A. R. Hendrix, T. H. Prettyman, C. A. Raymond, C. T. Russell, B. E. Sherwood, E. Young, Ceres: Astrobiological target and possible ocean world. *Astrobiology* **20**, 269–291 (2020).
14. A. Clarke, G. J. Morris, F. Fonseca, B. J. Murray, E. Acton, H. C. Price, A low temperature limit for life on Earth. *PLOS ONE* **8**, e66207 (2013).
15. M. C. De Sanctis, E. Ammannito, F. G. Carrozzo, M. Ciarniello, S. De Angelis, M. Ferrari, A. Frigeri, A. Raponi, Ammonium-rich bright areas on Ceres demonstrate complex chemical activity. *Commun. Earth Environ.* **5**, 131 (2024).
16. A. Raponi, M. C. De Sanctis, F. G. Carrozzo, M. Ciarniello, J. C. Castillo-Rogez, E. Ammannito, A. Frigeri, A. Longobardo, E. Palomba, F. Tosi, F. Zambon, C. A. Raymond, C. T. Russell, Mineralogy of Occator crater on Ceres and insight into its evolution from the properties of carbonates, phyllosilicates, and chlorides. *Icarus* **320**, 83–96 (2019).
17. J. Castillo-Rogez, P. Bland, "Ceres' Internal Evolution," in *Vesta and Ceres: Insights from the Dawn Mission for the Origin of the Solar System*, C. A. Raymond, C. T. Russell, S. Marchi, Eds. (Cambridge Univ. Press, 2022; www.cambridge.org/core/books/vesta-and-ceres/ceres-internal-evolution/4EFD4D6C58B317119F3DF04549AF03F1), pp. 159–172.
18. S. Marchi, A. Raponi, T. H. Prettyman, M. C. De Sanctis, J. Castillo-Rogez, C. A. Raymond, E. Ammannito, T. Bowling, M. Ciarniello, H. Kaplan, E. Palomba, C. T. Russell, V. Vinogradoff, N. Yamashita, An aqueously altered carbon-rich Ceres. *Nat. Astron.* **3**, 140–145 (2019).
19. T. J. Bowling, B. C. Johnson, S. Marchi, M. C. De Sanctis, J. C. Castillo-Rogez, C. A. Raymond, An endogenic origin of cerean organics. *Earth Planet. Sci. Lett.* **534**, 116069 (2020).
20. L. Chimiak, J. Eiler, Prebiotic synthesis on meteorite parent bodies: Insights from hydrogen and carbon isotope models. *Chem. Geol.* **644**, 121828 (2024).
21. J. Diab, M. M. Daswani, J. Castillo-Rogez, Bulk composition and thermal evolution constrain the formation of organics in Ceres' subsurface ocean via geochemical modeling. *Icarus* **391**, 115339 (2023).
22. N. G. Randolph-Flagg, T. Ely, S. M. Som, E. L. Shock, C. R. German, T. M. Hoehler, Phosphate availability and implications for life on ocean worlds. *Nat. Commun.* **14**, 2388 (2023).
23. C. F. Chyba, K. P. Hand, Life Without Photosynthesis. *Science* **292**, 2026–2027 (2001).
24. C. S. Cockell, M. Simons, J. Castillo-Rogez, P. M. Higgins, L. Kaltenegger, J. T. Keane, E. J. Leonard, K. L. Mitchell, R. S. Park, S. M. Perl, S. D. Vance, Sustained and comparative habitability beyond Earth. *Nat. Astron.* **8**, 30–38 (2024).
25. C. S. Cockell, T. Bush, C. Bryce, S. Direito, M. Fox-Powell, J. P. Harrison, H. Lammer, H. Landenmark, J. Martin-Torres, N. Nicholson, L. Noack, J. O'Malley-James, S. J. Payler, A. Rushby, T. Samuels, P. Schwendner, J. Wadsworth, M. P. Zorzano, Habitability: A review. *Astrobiology* **16**, 89–117 (2016).
26. E. L. Shock, M. E. Holland, Quantitative Habitability. *Astrobiology* **7**, 839–851 (2007).
27. J. Castillo-Rogez, B. Weiss, C. Beddingfield, J. Biersteker, R. Cartwright, A. Goode, M. Melwani Daswani, M. Neveu, Compositions and interior structures of the large moons of Uranus and implications for future spacecraft observations. *J. Geophys. Res. Planets* **128**, e2022JE007432 (2023).
28. D. Takir, J. P. Emery, H. Y. Mcsween Jr., C. A. Hibbitts, R. N. Clark, N. Pearson, A. Wang, Nature and degree of aqueous alteration in CM and CI carbonaceous chondrites. *Meteorit. Planet. Sci.* **48**, 1618–1637 (2013).
29. M. Neveu, S. J. Desch, Geochemistry, thermal evolution, and cryovolcanism on Ceres with a muddy ice mantle. *Geophys. Res. Lett.* **42**, 10,197–10,206 (2015).
30. J. C. Castillo-Rogez, T. B. McCord, Ceres' evolution and present state constrained by shape data. *Icarus* **205**, 443–459 (2010).
31. T. M. McCollom, Methanogenesis as a potential source of chemical energy for primary biomass production by autotrophic organisms in hydrothermal systems on Europa. *J. Geophys. Res. Planets* **104**, 30729–30742 (1999).
32. J. S. Seewald, M. Y. Zolotov, T. McCollom, Experimental investigation of single carbon compounds under hydrothermal conditions. *Geochim. Cosmochim. Acta* **70**, 446–460 (2006).
33. C. Ray, C. R. Glein, J. H. Waite, B. Teolis, T. Hoehler, J. A. Huber, J. Lunine, F. Postberg, Oxidation processes diversify the metabolic menu on Enceladus. *Icarus* **364**, 114248 (2021).
34. T. M. Hoehler, B. B. Jørgensen, Microbial life under extreme energy limitation. *Nat. Rev. Microbiol.* **11**, 83–94 (2013).
35. L. Tijhuis, M. C. M. Van Loosdrecht, J. J. Heijnen, A thermodynamically based correlation for maintenance gibbs energy requirements in aerobic and anaerobic chemotrophic growth. *Biotechnol. Bioeng.* **42**, 509–519 (1993).
36. S. W. Courville, J. C. Castillo-Rogez, M. M. Daswani, E. Gloesener, M. Choukroun, J. G. O'Rourke, Timing and abundance of clathrate formation control ocean evolution in outer solar system bodies: Challenges of maintaining a thick ocean within Pluto. *Planet Sci. J.* **4**, 179 (2023).
37. F. Piccoli, J. Hermann, T. Pettke, J. A. D. Connolly, E. D. Kempf, J. F. Vieira Duarte, Subducting serpentinites release reduced, not oxidized, aqueous fluids. *Sci. Rep.* **9**, 19573 (2019).
38. B. Debret, D. A. Sverjensky, Highly oxidising fluids generated during serpentinite breakdown in subduction zones. *Sci. Rep.* **7**, 10351 (2017).
39. B. B. Jørgensen, Shrinking majority of the deep biosphere. *Proc. Natl. Acad. Sci. U.S.A.* **109**, 15976–15977 (2012).
40. A. T. Fisher, K. L. Dickerson, D. K. Blackman, N. G. Randolph-Flagg, C. R. German, C. Sotin, Sustaining hydrothermal circulation with gravity relevant to ocean worlds. *J. Geophys. Res. Planets* **129**, e2023JE008202 (2024).
41. G. Choblet, G. Tobie, C. Sotin, M. Běhounková, O. Čadek, F. Postberg, O. Souček, Powering prolonged hydrothermal activity inside Enceladus. *Nat. Astron.* **1**, 841–847 (2017).
42. D. S. Kelley, J. A. Karson, G. L. Früh-Green, D. R. Yoerger, T. M. Shank, D. A. Butterfield, J. M. Hayes, M. O. Schrenk, E. J. Olson, G. Proskurowski, M. Jakuba, A. Bradley, B. Larson, K. Ludwig, D. Glickson, K. Buckman, A. S. Bradley, W. J. Brazelton, K. Roe, M. J. Elend, A. Delacour, S. M. Bernasconi, M. D. Lilley, J. A. Baross, R. E. Summons, S. P. Sylva, A serpentinite-hosted ecosystem: The Lost City hydrothermal field. *Science* **307**, 1428–1434 (2005).
43. S. W. Courville, J. G. O'Rourke, J. C. Castillo-Rogez, R. R. Fu, R. Oran, B. P. Weiss, L. T. Elkins-Tanton, Acquisition and preservation of remanent magnetization in carbonaceous asteroids. *Nat. Astron.* **6**, 1387–1397 (2022).
44. S. Vance, J. Harnmeijer, J. Kimura, H. Hussmann, B. DeMartin, J. M. Brown, Hydrothermal systems in small ocean planets. *Astrobiology* **7**, 987–1005 (2007).
45. B. R. Morton, G. Taylor, J. S. Turner, Turbulent gravitational convection from maintained and instantaneous sources. *Proc. R. Soc. Lond. A Math. Phys. Sci.* **234**, 1–23 (1956).
46. M. A. Hesse, J. S. Jordan, S. D. Vance, A. V. Oza, Downward oxidant transport through Europa's ice shell by density-driven brine percolation. *Geophys. Res. Lett.* **49**, e2021GL095416 (2022).
47. E. Carnahan, S. D. Vance, M. A. Hesse, B. Journaux, C. Sotin, Dynamics of mixed clathrate-ice shells on ocean worlds. *Geophys. Res. Lett.* **49**, e2021GL097602 (2022).
48. K. P. Hand, R. W. Carlson, C. F. Chyba, Energy, chemical disequilibrium, and geological constraints on Europa. *Astrobiology* **7**, 1006–1022 (2007).
49. S. D. Vance, K. P. Hand, R. T. Pappalardo, Geophysical controls of chemical disequilibria in Europa. *Geophys. Res. Lett.* **43**, 4871–4879 (2016).
50. H. Hiesinger, S. Marchi, N. Schmedemann, P. Schenk, J. H. Pasckert, A. Neesemann, D. P. O'Brien, T. Kneissl, A. I. Ermakov, R. R. Fu, M. T. Bland, A. Nathues, T. Platz, D. A. Williams, R. Jaumann, J. C. Castillo-Rogez, O. Ruesch, B. Schmidt, R. S. Park, F. Preusker, D. L. Buczkowski, C. T. Russell, C. A. Raymond, Cratering on Ceres: Implications for its crust and evolution. *Science* **353**, aaf4759 (2016).
51. J. F. Sauvage, A. Flinders, A. J. Spivack, R. Pockalny, A. G. Dunlea, C. H. Anderson, D. C. Smith, R. W. Murray, S. D'Hondt, The contribution of water radiolysis to marine sedimentary life. *Nat. Commun.* **12**, 1297 (2021).
52. T. Altair, M. G. B. de Avellar, F. Rodrigues, D. Galante, Microbial habitability of Europa sustained by radioactive sources. *Sci. Rep.* **8**, 260 (2018).

53. T. Altair, L. M. Sartori, F. Rodrigues, M. G. B. de Avellar, D. Galante, Natural radioactive environments as sources of local disequilibrium for the emergence of life. *Astrobiology* **20**, 1489–1497 (2020).
54. R. Ribeiro de Sousa, A. Morbidelli, R. Gomes, E. V. Neto, A. Izidoro, A. A. Alves, Dynamical origin of the dwarf planet Ceres. *Icarus* **379**, 114933 (2022).
55. S. J. Desch, A. Kalyaan, C. M. O. Alexander, The effect of Jupiter's formation on the distribution of refractory elements and inclusions in meteorites. *Astrophys. J. Suppl. Ser.* **238**, 11 (2018).
56. M. Y. Zolotov, The composition and structure of Ceres' interior. *Icarus* **335**, 113404 (2020).
57. B. Reynard, C. Sotin, Carbon-rich icy moons and dwarf planets. *Earth Planet. Sci. Lett.* **612**, 118172 (2023).
58. J. C. Castillo, M. M. Daswani, S. W. Courville, "Consequences of large abundances of organic matter on the habitability potential of icy moons and dwarf planets," in *2024 Astrobiology Science Conference* (AGU, 2024).
59. T. D. Ely, J. M. Leong, P. A. Canovas, E. L. Shock, Huge variation in H_2 generation during seawater alteration of ultramafic rocks. *Geochem. Geophys. Geosyst.* **24**, e2022GC010658 (2023).
60. National Academies of Sciences and Medicine, *Origins, worlds, and life: a decadal strategy for planetary science and astrobiology 2023–2032* (The National Academies Press, 2022).
61. M. E. Zolensky, R. J. Bodnar, H. Yurimoto, S. Itoh, M. Fries, A. Steele, Q. H.-S. Chan, A. Tsuchiyama, Y. Kebukawa, M. Ito, The search for and analysis of direct samples of early Solar System aqueous fluids. *Philos. Trans. A Math. Phys. Eng. Sci.* **375**, 20150386 (2017).
62. C. A. de Moura, C. S. Kubrusly, *The Courant–Friedrichs–Lewy (CFL) Condition: 80 Years After Its Discovery* (Birkhäuser Boston, 2012); https://books.google.com/books?id=XXiNMQEACAAJ.
63. S.-C. Han, N. Schmerr, G. Neumann, S. Holmes, Global characteristics of porosity and density stratification within the lunar crust from GRAIL gravity and Lunar Orbiter Laser Altimeter topography data. *Geophys. Res. Lett.* **41**, 1882–1889 (2014).
64. W. Neumann, D. Breuer, T. Spohn, Modelling of compaction in planetesimals★. *Astron. Astrophys.* **567**, 15 (2014).
65. K. Kalousová, C. Sotin, Dynamics of Titan's high-pressure ice layer. *Earth Planet. Sci. Lett.* **545**, 116416 (2020).
66. W. Neumann, R. Jaumann, J. Castillo-Rogez, C. A. Raymond, C. T. Russell, Ceres' partial differentiation: undifferentiated crust mixing with a water-rich mantle. *Astron. Astrophys.* **633**, 27 (2020).
67. H. Palme, J. Zipfel, The composition of CI chondrites and their contents of chlorine and bromine: Results from instrumental neutron activation analysis. *Meteorit. Planet. Sci.* **57**, 317–333 (2022).
68. K. Lodders, "Solar system abundances of the elements," in *Principles and Perspectives in Cosmochemistry: Lecture Notes of the Kodai School on'Synthesis of Elements in Stars' Held at Kodaikanal Observatory, India, April 29-May 13, 2008* (Springer, 2010), pp. 379–417.
69. M. J. Mayne, J.-F. Moyen, G. Stevens, L. Kaislaniemi, Rcrust: A tool for calculating path-dependent open system processes and application to melt loss. *J. Metam. Geol.* **34**, 663–682 (2016).
70. J. A. D. Connolly, The geodynamic equation of state: What and how. *Geochem. Geophys. Geosyst.* **10**, Q10014 (2009).
71. R. G. BERMAN, Internally-Consistent Thermodynamic Data for Minerals in the System Na_2O-K_2O-CaO-MgO-FeO-Fe_2O_3-Al_2O_3-SiO_2-TiO_2-H_2O-CO_2. *J. Petrol.* **29**, 445–522 (1988).
72. T. J. B. HOLLAND, R. POWELL, An improved and extended internally consistent thermodynamic dataset for phases of petrological interest, involving a new equation of state for solids. *J. Metam. Geol.* **29**, 333–383 (2011).
73. S. Goes, D. Hasterok, D. L. Schutt, M. Klöcking, Continental lithospheric temperatures: A review. *Phys. Earth Planet. In.* **306**, 106509 (2020).
74. J. A. D. CONNOLLY, B. CESARE, C-O-H-S fluid composition and oxygen fugacity in graphitic metapelites. *J. Metam. Geol.* **11**, 379–388 (1993).
75. C. M. Bethke, *Geochemical and Biogeochemical Reaction Modeling* (Cambridge Univ. Press, ed. 2, 2007; www.cambridge.org/core/books/geochemical-and-biogeochemical-reaction-modeling/A5688B8238EAF9F61568645A88FC9E2C).
76. T. J. Wolery, "EQ3/6, a software package for geochemical modeling of aqueous systems: Package overview and installation guide (Version 7.0)" (1992); https://doi.org/10.2172/138894.
77. J. W. Johnson, E. H. Oelkers, H. C. Helgeson, SUPCRT92: A software package for calculating the standard molal thermodynamic properties of minerals, gases, aqueous species, and reactions from 1 to 5000 bar and 0 to 1000°C. *Comput. Geosci.* **18**, 899–947 (1992).
78. M. Rubin, K. Altwegg, H. Balsiger, J.-J. Berthelier, M. R. Combi, J. De Keyser, M. Drozdovskaya, B. Fiethe, S. A. Fuselier, S. Gasc, T. I. Gombosi, N. Hänni, K. C. Hansen, U. Mall, H. Rème, I. R. H. G. Schroeder, M. Schuhmann, T. Sémon, J. H. Waite, S. F. Wampfler, P. Wurz, Elemental and molecular abundances in comet 67P/Churyumov-Gerasimenko. *Mon. Not. R. Astron. Soc.* **489**, 594–607 (2019).
79. J. T. Romero, "Changes in microbial communities and geochemical energy supplies across the photosynthetic fringe of hot spring outflows in Yellowstone National Park," thesis, Arizona State University, Tempe, AZ (2018).
80. E. Ortega-Arzola, P. M. Higgins, C. S. Cockell, The minimum energy required to build a cell. *Sci. Rep.* **14**, 5267 (2024).
81. C. R. Glein, M. Y. Zolotov, E. L. Shock, The oxidation state of hydrothermal systems on early Enceladus. *Icarus* **197**, 157–163 (2008).
82. W. F. Giggenbach, Relative importance of thermodynamic and kinetic processes in governing the chemical and isotopic composition of carbon gases in high-heatflow sedimentary basins. *Geochim. Cosmochim. Acta* **61**, 3763–3785 (1997).
83. S. Courville, WOW! v0.9 (Zenodo, 2025); 10.5281/zenodo.15306344.

Acknowledgments: We thank E. Shock for many helpful discussions during the preparation of this work. This research was carried out at Arizona State University and the Jet Propulsion Laboratory, California Institute of Technology, under a contract with the NASA (80NM0018D0004) and funding from the Habitable Worlds program. Government sponsorship is acknowledged. **Funding:** This research was funded by NASA Habitable Worlds grant 80NM0018D0004 (to J.C.C.-R.). **Author contributions:** Conceptualization: S.W.C., J.C.C.-R., and M.M.D. Methodology: S.W.C., J.R., J.C.C.-R., and M.M.D. Investigation: S.W.C. Visualization: S.W.C. Supervision: J.C.C.-R., M.M.D., and J.G.O. Resources: M.M.D. Validation: M.M.D. Formal analysis: M.M.D. Software: M.M.D. Writing—original draft: S.W.C., J.C.C.-R., and M.M.D. Writing—review and editing: S.W.C., J.C.C.-R., M.M.D., J.G.O., and J.R. **Competing interests:** The authors declare that they have no competing interests. **Data and materials availability:** All data needed to evaluate the conclusions in the paper are present in the paper and/or the Supplementary Materials. The code that generated the results are freely available on Github at https://github.com/SamuelCourville/WOW and in an archived version at the time of publication (*83*).

Submitted 23 September 2024
Accepted 24 July 2025
Published 20 August 2025
10.1126/sciadv.adt3283